LAWRENCE
LIVERMORE
NATIONAL
LABORATORY

UCRL-JRNL-219074

The Thermal Stability of Nanocrystalline Au-Cu Alloys

A. F. Jankowski, C. K. Saw, J. P. Hayes

February 16, 2006

Thin Solid Films

The thermal stability of nanocrystalline Au-Cu alloys

Alan F. Jankowski, Cheng K. Saw, and Jeffrey P. Hayes

Chemistry and Materials Science, Materials Science and Technology Division
Lawrence Livermore National Laboratory, P.O. Box 808, MS L-352,
Livermore, CA 94550 USA

Abstract

Grain refinement to the nanocrystalline scale is known to enhance physical properties as strength and surface hardness. For the case of Au-Cu alloys, development of the pulsed electroplating has led to the functional control of nanocrystalline grain size in the as-deposited condition. The thermal aging of Au-Cu electrodeposits is now investigated to assess the stability of the nanocrystalline grain structure and the difference between two diffusion mechanisms. The mobility of grain boundaries, dominant at low temperatures, leads to coarsening of grain size whereas at high temperature the process of bulk diffusion dominates. Although the kinetics of bulk diffusion are slow below 500 K at 10^{-20} $cm^2 \cdot sec$, the kinetics of grain boundary diffusion are faster at 10^{-16} $cm^2 \cdot sec$. The diffusivity values indicate that the grain boundaries of the as-deposited nanocrystalline Au-Cu are mobile and sensitive to low-temperature anneal treatments affecting the grain size, hence the strength of the material.

Introduction

Nanocrystalline foils of Au-Cu alloys [1-2] can be produced by electrodeposition processes. The process of pulsed electrodeposition provides a path to control the as-deposited grain size, e.g. of nanocrystalline $Au_{1-x}Cu_x$ alloys [3]. The electrodeposition parameters of cell

potential, current density, and pulse duration are modeled [4] to the measurements of the crystallite size within the Au-Cu foil. By modifying the pulse conditions, different grain sizes can be produced at the same alloy composition in the as-deposited structure. The refinement of grain size provides a means to increase the strength of materials according to the well-known Hall-Petch relationship. In general, the hardness of metals and alloys is known [5-6] to increase with grain refinement from the micro-to-nanocrystalline scale. Values of tensile strength for electrodeposited Au-Cu alloys have been reported [7] an order of magnitude greater than that of ~100 MPa value normally associated with fully-annealed solid solutions. Mechanically testing evidence obtained for alloys after thermal anneal treatments associates increased strength to the formation of Au-Cu intermetallic phases [8] having coherency strains with the disordered Au-Cu matrix. The Au-Cu intermetallic phases include $AuCu_3$, AuCu, and Au_3Cu [9] with typical activation energies of 0.8 to 1 $eV \cdot atom^{-1}$. Ordering from the disordered Au-Cu solution takes place at temperatures within the miscibility gap, that is, generally below 673 K. Also, as is the general case for nanocrystalline metal alloys with low melting temperature, the grain size is quite sensitive to anneal treatments.

In this study, the kinetics of grain boundary diffusion at low temperature is determined from grain growth as measured using x-ray diffraction. A comparison to the assessment of bulk diffusion kinetics in Au-Cu foils at low temperatures is made through the use of concentration waves [10] and the microscopic theory [11] of diffusion. This reference approach provides a low-temperature benchmark for bulk diffusion kinetics [12] normally associated with the high-temperature mobility of the Au^{198} tracer isotope in Cu [13] and Au [14]. Also, since grain size coarsening of nanocrystalline Au-Cu foils at low temperature is anticipated, a path to stabilize the nanostructure of the binary Au-Cu alloy is proposed through the addition of a metal with a dissimilar crystallographic structure. We will assess the effect on grain size stability for the

addition of a body-centered-cubic (bcc) additive as tin (Sn) to the host face-centered-cubic (fcc) structure of the disordered Au-Cu alloy creating a pseudobinary Au(Cu)-Sn alloy [15].

Experimental and Analysis Methods

The electrodeposition process to produce free-standing Au-Cu foils with 1-20 wt.% Cu has been described in detail [3]. In brief, a 1.5 liter cyanoalkaline solution is used to electroplate a 10-20 μm thick Au-Cu foil onto a 12 cm^2 substrate of titanium. The foil is easily removed from the substrate and cut into 1 cm^2 pieces for composition determination and vacuum anneal treatments. The energy dispersive x-ray spectra of the free standing foils reveal the characteristic Cu *L*, Au *M*, and Sn *L* x-ray peaks that are used to quantify the composition as determined from the atomic number (Z)–absorption (A)–fluorescence (F) semi-quantitative analysis. A base pressure less than 0.1 mPa is maintained throughout the anneal cycle by cryogenic pumping. Within each anneal treatment, the sample is held at peak temperature (T) for 30 minutes. The peak temperature range for the anneal treatments are: 478-503 K (A_1); 568-598 K (A_2); 671-713 K (A_3); and 741-805 K (A_4). The process temperature during deposition (A_0) was 293-338 K.

The method of x-ray diffraction provides a means to measure the grain size (d_g) as determined through broadening of Bragg reflections seen in Cu K_α x-ray diffraction scans taken in the θ/2θ mode. The grain size (d_g) is quantified using the Debye-Scherrer formulation [16] as,

$$d_g = 0.9 \cdot \lambda \cdot (B \cdot \cos\theta)^{-1} \qquad (1)$$

where λ is the x-ray wavelength (equal to 0.1542 nm for Cu K_α x-rays), and 2θ is the position of the Bragg reflection with peak intensity. The formulation [16] to correct the measured full-width (B_m) at half-maximum intensity of the Bragg reflection for instrument broadening (B_s) is,

$$B^2 = B_m^2 - B_s^2 \quad (2)$$

where the Bragg peak is fit with a Gaussian distribution.

A relationship to compute the activation energy for grain growth [17] during isothermal anneal treatments is found in the grain growth law. Grain size, as determined from equations (1-2), is proportional to the anneal time (t) raised to the power n, i.e. $d_g \alpha t^n$. For the case of ideal grain growth, the exponent n equals 0.5. This is typically observed, as reported [18] for coarsening of grain size in Al foils. Thus, the change in grain size (Δd_g) with anneal time is,

$$[\Delta d_g]^2 = [d_g(f)]^2 - [d_g(i)]^2 \quad (3)$$

where $d_g(i)$ is the as-deposited grain size and $d_g(f)$ is the final grain size. A linear variation of T^{-1} versus $\ln(\Delta d_g^2 \cdot t^{-1})$ follows [17-19] when the evolution of grain size with time at temperature follows ideal grain growth. The slope of the linear variation yields an activation energy (Q) representative of the diffusion mechanism. High and low temperature regimes [20-22] are typical for bulk versus grain boundary diffusion, respectively. A linear regression analysis of the data provides the activation energy (Q) from the relationship,

$$Q = -R \cdot \partial[\ln \check{D}] \cdot \partial[T^{-1}]^{-1} \quad (4)$$

where R is the molar gas constant (8.314 $J \cdot mol^{-1} \cdot K^{-1}$) and the diffusivity ($\check{D}$) equals ($\Delta d_g^2 \cdot t^{-1}$).

Results

Nanocrystalline Size and Stability

The vacuum anneal treatments coarsen the nanocrystalline grain size of the as-deposited structure. The time (t) at temperature (T) plots of the anneal treatments for the 18 wt.% Cu foils of sample set no. 1 are shown in Fig. 1. Each foil is annealed from its as-deposited condition as

opposed to successive anneal treatments of one specimen at increasing temperature. For the analysis of grain size, the initial grain size $d_g(i)$ is equal to that value measured for the A_0 condition whereas $d_g(f)$ equals the value measured after each A_n anneal treatment.

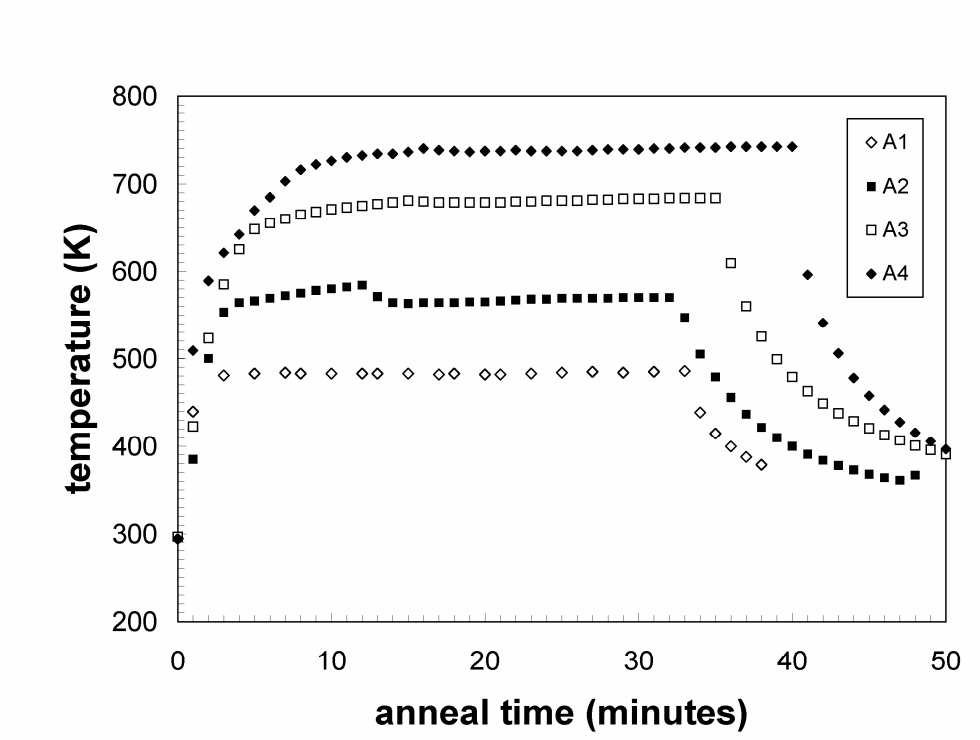

Figure 1. The time-at-temperature history of the A_1 through A_4 vacuum-anneal treatments for the Au-18 wt.% Cu sample set no. 1.

The Au-Cu electrodeposited samples are polycrystalline as seen in the x-ray diffraction scans of Fig. 2 for the 18 wt.% Cu example. For reference, the common powder diffraction files for face-centered-cubic (fcc) Au indicate a lattice parameter of 0.4079 nm, and 0.3615 nm for fcc Cu. In this study, all of the Au-Cu foils in the as-deposited condition contain the fundamental reflections that correlate with composition weighted averages. This result indicates electrodeposited foils are equiaxed fcc polycrystals. There is no evidence for textured film growth from the x-ray diffraction scans. The lattice parameters of the ordered intermetallics are 0.3749 nm for cubic $AuCu_3$ (PDF no. 35-1357), 0.396 nm (a=b) and 0.367 nm (c) for tetragonal AuCu (PDF no. 25-1220), and 0.4088 nm for cubic Au_3Cu (PDF no. 34-1302).

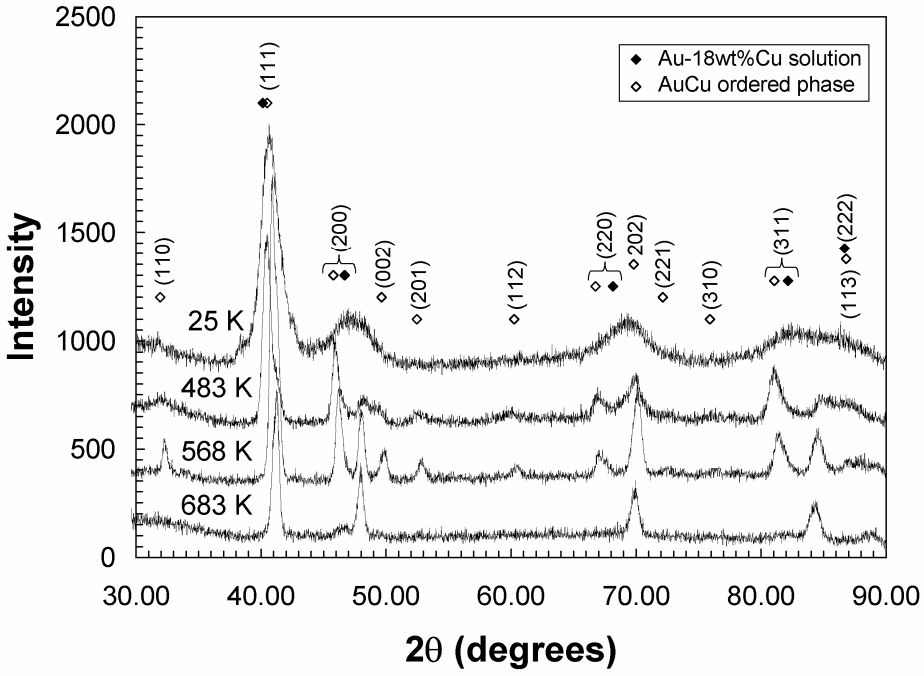

Figure 2. Au-18 wt.% Cu x-ray diffraction scans taken using Cu $K\alpha$ radiation in the θ/2θ mode as-deposited and after the 30-minute A_1 through A_3 anneal treatments.

The Bragg reflections that correspond to the disordered Au-18 wt.% Cu phase and the ordered AuCu phase are labeled in Fig. 2 for reference. As the foils are annealed at temperatures within the miscibility gap, i.e. below 683 K for the 18 wt.% Cu set, ordering from the disordered fcc solid solution to that of a mixed phase with the presence of the AuCu ordered phase is seen in the diffraction patterns of Fig. 2. At or above 683 K, i.e. above the miscibility gap, the disordered solution remains the only phase present in the foil. These results are consistent with the Au-Cu phase diagram [9] wherein an ordered phase of AuCu forms in $Au_{1-x}Cu_x$ where $17< x <35$ wt.% Cu. A maximum decomposition temperature of 683 K at ~24 wt.% Cu decreases to only 523 K at 17 wt.% Cu. For all samples, it can be seen that the full width at half maximum intensity of the (111) Bragg reflection decreases with increasing anneal temperature.

Table I. Grain size d_g (nm) after each anneal treatment (A_n) and the corresponding activation energy Q (eV·atom^{-1}) for growth in $Au_{1-x}Cu_x$ foils of composition x (wt.% Cu)

Sample Set	x (wt.% Cu)	d_g (nm)					Q (eV·atom^{-1})
		A_0	A_1	A_2	A_3	A_4	
1	18	5.4	10.6	12.6	15.8	24.1	0.139
2	14	6.2	8.0	9.4	10.9	14.9	0.174
4	12	5.5	11.2	14.7	19.3	27.8	0.183
5	12	7.7	11.8	15.4	19.1	-	0.214
6	4	31.2	40.9	51.9	65.0	94.3	0.207
8	4	10.3	12.9	14.3	17.9	23.2	0.186

The Bragg reflection with the greatest peak intensity, i.e. the (111), is used to determine grain size (d_g) from equations (1-2) and the diffraction scans. We measure B_s as 0.19° (2θ) for a single-crystal reference sample of Au (111). The as-deposited $d_g(i)$ and $d_g(f)$ after each nominal 30-minute anneal treatment (A_n) are listed in Table 1 for each Au-Cu sample set. The nominal composition for each foil is listed as determined [3] to within ±1 wt.% from the energy dispersive x-ray analysis. For all samples, it is seen that the grain size computed using the (111) Bragg reflection increases with increasing anneal temperature.

To assess stabilization of nanocrystalline Au-Cu through an alloy addition, Sn was added to the standard bath [3] used for Au-Cu electrodeposition. In this case, the 1500 ml solution bath was composed of 15 gm KCN, 20 gm $KCu(CN)_2$, 5 gm $KAu(CN)_2$, 10 gm $SnCl_4{\cdot}5H_2O$, and 7 gm NaOH. A sample with a 32 wt.% Cu-4 wt.% Sn composition was produced as determined by energy dispersive x-ray spectroscopy. X-ray diffraction scans are shown in Fig. 3 for the as-deposited condition and after the A_1-A_3 anneal treatments. As seen for the case of the 18 wt.% Cu foils in Fig. 2, the samples are polycrystalline and evidence ordering at the lower anneal

temperatures (of 480 K and 603 K in this case). For the 703 K anneal, the specimen appears to be a single-phase disordered solid solution. This diffraction pattern matches the result reported [15] for the disordered phase seen in low Sn-alloy compositions of the Au(Cu)-Sn pseudobinary. The Bragg reflections that correspond to Au, Cu, AuCu, and the disordered pseudobinary 32 wt.% Cu-4 wt.% Sn phases are labeled in Fig. 3 for reference. The x-ray patterns we see in Fig. 3 for the 480 K and 603 K anneal conditions exhibit the type of ordering associated with the AuCu phase as well, and the AuCu III phase – an orthorhombic variant of AuCu. The characteristic 2θ reflection for AuCu III is seen at 42.3º and is reported [15] as present up to a ~600K anneal temperature.

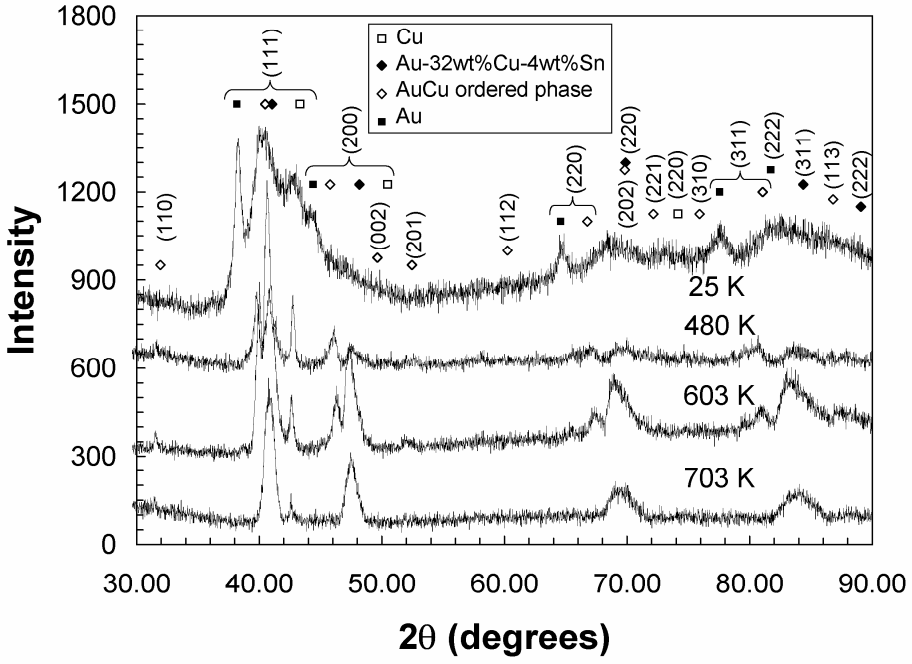

Figure 3. Au-32 wt.% Cu-4 wt.% Sn x-ray diffraction scans taken using Cu $K\alpha$ radiation in the θ/2θ mode as-deposited and after the 30-minute A_1 through A_3 anneal treatments.

Although remaining nanocrystalline, the addition of Sn does not completely stabilize the small 3 nm as-deposited grain size $d_g(i)$. The 703 K anneal increases d_g to 8.8 nm. However, this d_g value is less than measured for all Au-Cu samples after an A_3 anneal treatment.

Diffusion and Activation Energy

The activation energy for diffusion (Q) is computed from the slope of the linear curves in the Fig. 4 Arrhenius plot of inverse temperature (T^{-1}) with the natural logarithm of diffusivity (ln Ď). The formulations to derive Q were previously discussed using equations (3-4). The Table 1 data for samples sets no. 1, 2, 4, and 6 are plotted in Fig. 4 as illustrative examples.

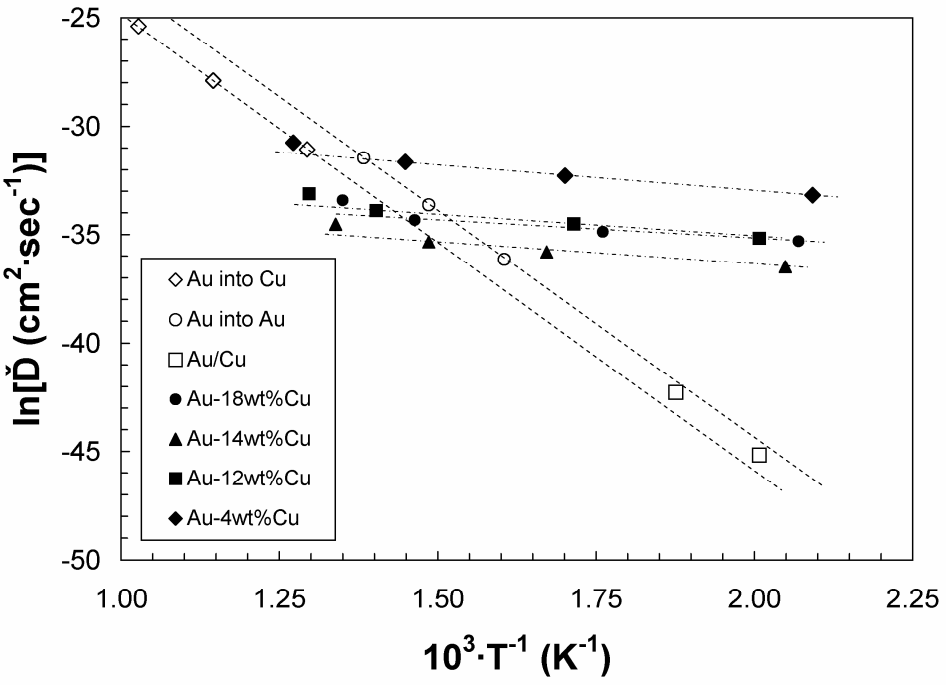

Figure 4. An Arrhenius plot of $10^3 \cdot T^{-1}$ (K^{-1}) versus ln[Ď ($cm^2 \cdot sec^{-1}$)] for Au-Cu samples. High-temperature isotope [13-14] and low-temperature nanolaminate [10, 12] data delineate the transition between grain boundary and bulk diffusion mechanisms.

The reference dashed curves represent the linear regression fit to high-temperature isotope diffusion of Au^{198} into Au [14] as well as Cu [13]. The corresponding activation energy

(Q_b) for bulk diffusion is ~1.8 eV·atom $^{-1}$ (175 kJ·mol^{-1}·K^{-1} or 42 kcal·mole^{-1}). The extrapolation to low temperature intercepts diffusivity values determined [12] from the decay of composition fluctuations in thermally-annealed Au/Cu nanolaminates [10]. The bulk diffusion fit provides a temperature reference as to where the transition in dominant diffusion mechanism takes place. For the Au-Cu samples, the transition from bulk to grain boundary diffusion occurs at ~670 K. That is, the grain boundary diffusion mechanism is dominant for anneal temperatures to the right of the bulk-diffusion reference curve. Grain boundary diffusivities are 10^{-14}-10^{-16} cm^2·sec^{-1} over this temperature range. At 500 K for instance, the diffusivity for bulk diffusion would be four orders of magnitude less at only 10^{-20} cm^2·sec^{-1}. The activation energy for grain boundary diffusion (Q_{gb}) is determined from a linear regression analysis of diffusivity values for anneal temperatures that lie to the right of the bulk-diffusion reference curve. The Q_{gb} values are listed for each Au-Cu sample set in Table 1. The Q_{gb} values range from 0.14-0.21 eV·atom^{-1} which is an order of magnitude less than for bulk diffusion at ~1.8 eV·atom^{-1}. Diffusivities determined from grain size coarsening above the temperature that corresponds with bulk diffusion deviate from the linear fit for grain boundary diffusion. These diffusivity data points lie above the grain boundary fit for each sample set. This indicates that as temperature exceeds the bulk-diffusion curve reference, the influence of the bulk diffusion mechanism now affects the diffusivity associated with grain size coarsening as it should be.

Discussion

The large difference between activation energies for high and low temperature regimes is in agreement with a compilation of findings by Martin and Perraillon [20]. They note for the case of self-diffusion, as approximated for by the Au-Cu case under study, that the apparent activation energy in a grain boundary is roughly half (or less) than the activation energy for bulk diffusion.

In reference to short-circuit diffusion networks, Harrison [22] notes three diffusion regimes that can be distinguished according to the bulk penetration depth being smaller than (regime B), roughly equal to (regime A), or larger (regime C) than a characteristic length of the network, e.g. the average grain size. Consequently, as in the case of Harrison's A regime, it may be inferred [22] that the effective diffusivity ($\check{D}_{eff}$) for grain growth can be considered attributable to the volume fraction (f) contribution of dislocations with respect to dislocation diffusion ($\check{D}_{disl}$) and volume (lattice) diffusion ($\check{D}_{vol}$). That is, an arithmetic rule-of-mixtures summation as

$$\check{D}_{eff} = (1-f)\cdot\check{D}_{vol} + f\cdot\check{D}_{disl} \qquad (5)$$

In general, the similarity of the present case exists over the broad temperature range examined wherein a transition from grain boundary to bulk diffusion occurs. More than one mechanism [23-24] contributes at temperatures above ~670 K. In this regard, a transition in the dominant diffusion mechanism from grain boundary to bulk occurs, above roughly half the melt temperature of the alloy.

The effect of grain size on mechanical strength, specifically tensile strength (σ) has been examined for microcrystalline Au and nanocrystalline Au-Cu alloys. This functional relationship provides a motivation for examining the stability of nanocrystalline grain size in with temperature. Typical results for uniaxial tensile tests [25] at strain rates of 10^{-5}-10^{-6} sec^{-1} are plotted in Fig. 5 for pure Au foils deposited by electron-beam evaporation. (This brief discussion is intended to generally assess the Hall-Petch relationship but not to differentiate the details of strain-rate sensitivity effects on strength mechanism.) The 240-280 MPa strength of foils with 0.2-0.4 μm decreases with an anneal treatment to ~100 MPa as the grains coarsen to 4 μm in size. Some recent results [26] for nanocrystalline $Au_{1-x}Cu_x$ ($12< x <19$ wt.% Cu) foils prepared by pulsed electrodeposition are plotted as well in Fig. 5. For comparison, these tensile tests are conducted at similar strain rates of 10^{-5} sec^{-1}. The foils are laser cut from sheet to yield a standard

tensile shape with a (1 cm) gage length to width ratio of 4:1. Upper bound values are plotted, as several samples were observed to fail prior to any plastic deformation. In general, an increase in strength is observed as grain size decreases to 6 nm. Tensile strengths as high as 1200 MPa (173 ksi) are reported [7] for electrodeposited Au-Cu foils heat treated (for 3 hrs. at 573 K) wherein it's shown that increasing the Cu composition (and the presence of Au-Cu intermetallic phases) greatly contribute to the high peak strengths.

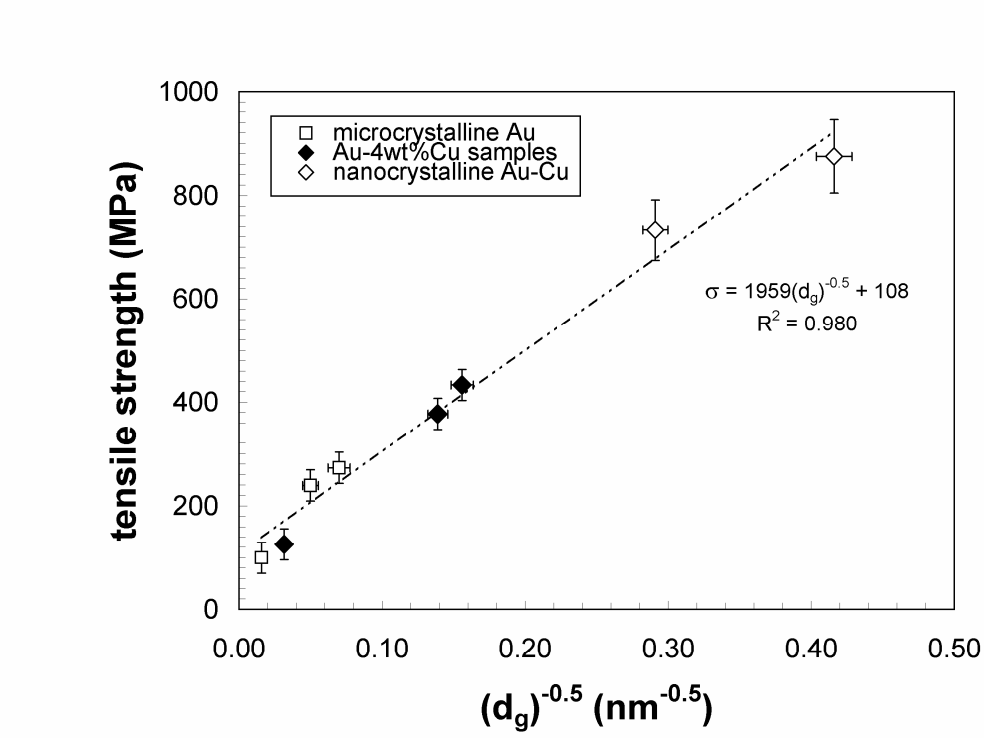

Figure 5. A Hall-Petch plot of grain size $d_g^{-0.5}$ ($nm^{-0.5}$) with strength σ (MPa) for Au [25], Au-Cu [26], and foils of the Au-4 wt.% Cu sample set no. 6.

In addition, a few preliminary test results are plotted in Fig. 5 for tensile specimens prepared from Au-Cu sample sets no. 6 and 8 with 4 wt.% Cu. In particular, the 377 and 433 MPa results are for the A_1 and A_2 samples of set no. 6, respectively. A fully annealed 1 μm grain-size Au-Cu sample at ~120 MPa is plotted as well in Fig. 5. The presence of only the disordered fcc Au-Cu structure was observed in the x-ray diffraction patterns for these tensile specimens from sample set no.6. The increase in strength with decreasing grain size indicates

that the presence of a nanocrystalline structure alone can greatly influence strength. For this case of a disordered fcc structure, the temperature sensitivity of the grain size to the thermal anneal treatment causes coarsening that results in the loss of peak strength. Further results and discussion of strength measurements will be presented in the future.

Summary

Electrodeposits of $Au_{1-x}Cu_x$ have been prepared and examined using x-ray diffraction. The stability of an as-deposited nanocrystalline grain size is assessed after thermal anneal treatments via peak broadening. A coarsening of grain size in nanocrystalline Au-Cu leads to decreased strength. A transition in the dominant mechanism for diffusion is observed above 670 K wherein bulk diffusion rates exceed the rates measured for grain boundaries. The increase of grain size with temperature is assessed using the grain growth law and yield diffusivity values ($\check{D}$) of 10^{-14}-10^{-16} $cm^2 \cdot sec^{-1}$ over the temperature range of 478-805 K. The activation energy (Q_{gb}) for grain growth in $Au_{1-x}Cu_x$ ranges from 0.14-0.21 eV atom and generally appears to decrease over this narrow range as the composition (x) increases from 4 to 18 wt.% Cu. The addition of Sn to the electrochemical bath yields a pseudobinary Au(Cu)-Sn phase of composition 32 wt.% Cu-4 wt.% Sn that appears to be less sensitive to grain size coarsening with anneal treatment than the Au-Cu binary alloy.

Acknowledgment

This work was performed under the auspices of the United States Department of Energy by the University of California, Lawrence Livermore National Laboratory under Contract No. W-7405-Eng-48.

References

1. B. Bozzini, G. Giovannelli, and P. Cavallotti, J. Appl. Electrochem., 29 (1999) 685

2. B. Bozzini and P.L. Cavalotti, J. Electrochem. Soc., 148 (2001) C231

3. A.F. Jankowski, C.K. Saw, J.F. Harper, R.F. Vallier, J.L. Ferreira, and J.P. Hayes, Thin Solid Films, 494 (2006) 268

4. A.F. Jankowski, Electrochem. Soc. Trans., 1 (2006) in press

5. R.W. Siegel, Mater. Sci. Forum, 235-238 (1997) 851

6. T.G. Nieh and J. Wadsworth, Scripta Metall. Mater., 25 (1991) 955

7. H.J. Wiesner and W.B. Distler, Plating, 56 (1969) 799

8. M. Hirabayashi and S. Weissmann, Acta Met., 10 (1962) 25

9. M. Hansen, in T.B. Massalski (ed.) Binary Alloy Phase Diagrams, Vol. 1, , ASM, Metals Park, Ohio,1986, p. 253

10. W.M. Paulson and J.E. Hilliard, J. Appl. Phys., 48 (1977) 2117

11. A.G. Khachaturyan, Theory of Structural Transformations in Solids, John Wiley and Sons, New York, 1983, pp. 128-136

12. A.F. Jankowski, C.K. Saw and J.S. Harper, TMS Letters, 2 (2) (2005) 55

13. A. Chatterjee, D.J. Fabian, Acta Mater., 17 (1969) 1141

14. H.M. Gilder and D. Lazarus, J. Phys. Chem. Solids, 26 (1965) 2081

15. C.N.C. Luciano, K. Udoh, M. Nakagawa, S. Matsuya, and M. Ohta, J. Alloys Compounds, 337 (2002) 289

16. B.D. Cullity, Elements of X-Ray Diffraction, Addison-Wesley Publ. Co., Reading, Massachusetts, 1978, pp. 101-3, 284-5

17. R.E. Reed-Hill, Physical Metallurgy Principles, Van Nostrand, New York, 1973, pp. 304-310

18. A.F. Jankowski, J.L. Ferreira, and J.P. Hayes, Thin Solid Films, 491 (2005) 61

19. P. Feltham and G.J. Copley, Acta Met., 6 (1958) 539

20. G. Martin and B. Perraillon, in Grain Boundary Structure and Kinetics, ASM Materials Science Seminar, ASM, Metals Park, Ohio, 1979, p. 239

21. E.W. Hart, Acta Metall., 5 (1957) 597

22. L.G. Harrison, Trans. Farad. Soc., 57 (1961) 1191

23. J.L. Bocquet, G. Brébee, and Y. Limoge, in R. W. Cahn and P. Haasen (eds.) Physical Metallurgy, 3rd edn., North Holland Physics Publishing, Amsterdam, 1983, pp. 403, 415

24. A. Seeger and H. Mehrer, in A. Seeger, D. Schumacher, and J. Diehl (eds.) Vacancies and Interstitials in Metals, North Holland, Amsterdam, 1970, p. 1

25. R.D. Emery and G.L. Povrik, Acta Mater., 51 (2003) 2079

26. Y.M. Wang, A.F. Jankowski, A.F. Hamza, in A.F. Hamza (ed.) 2005 Annual Report of the Nanoscale Synthesis and Characterization Laboratory, UCRL-TR-217985, Lawrence Livermore National Laboratory, Livermore, CA, 2006, p. 11